10-2021

Anchor Self-Calibrating Schemes for UWB based Indoor Localization

Jonathan Pereira
jp6697@rit.edu

Anchor Self-Calibrating Schemes for UWB based Indoor Localization

Jonathan Pereira

Anchor Self-Calibrating Schemes for UWB based Indoor Localization

Jonathan Pereira

October 2021

A Thesis Submitted
in Partial Fulfillment
of the Requirements for the Degree of
Master of Science
in
Computer Engineering

RIT | Kate Gleason College of Engineering

Department of Computer Engineering

Anchor Self-Calibrating Schemes for UWB based Indoor Localization

Jonathan Pereira

Committee Approval:

Dr. Tae Oh *Advisor* Date
School of Information

Dr. Andres Kwasinski *Committee Member* Date
Department of Computer Engineering

Dr. Amlan Ganguly *Committee Member* Date
Department of Computer Engineering

Acknowledgments

I would like to thank my advisor Dr. Tae Oh for his advice and support with my academics and this thesis. I would also like to express my gratitude to Dr. Andres Kwasinski and Dr. Amlan Ganguly for being a part of my thesis committee. I would also like to thank my family and friends for their continuous encouragement and support all through my studies.

Abstract

Traditional indoor localization techniques that use Received Signal Strength or Inertial Measurement Units for dead-reckoning suffer from signal attenuation and sensor drift, resulting in inaccurate position estimates. Newly available Ultra-Wideband radio modules can measure distances at a centimeter-level accuracy while mitigating the effects of multipath propagation due to their very fine time resolution. Known locations of fixed anchor nodes are required to determine the position of tag nodes within an indoor environment. For a large system consisting of several anchor nodes spanning a wide area, physically mapping out the locations of each anchor node is a tedious task and thus makes the scalability of such systems difficult. Hence it is important to develop indoor localization systems wherein the anchors can self-calibrate by determining their relative positions in Euclidean 3D space with respect to each other.

In this thesis, we propose two novel anchor self-calibrating algorithms - Triangle Reconstruction Algorithm (TRA) and Channel Impulse Response Positioning (CIR-Pos) that improve upon existing range-based implementations and solve existing problems such as flip ambiguity and node localization success rate. The localization accuracy and scalability of the self-calibrating anchor schemes are tested in a simulated environment based on the ranging accuracy of the Ultra-Wideband modules.

Contents

List of Figures

List of Tables

Chapter 1

Introduction

.

Global Positioning Systems (GPS) have achieved wide-scale adoption due to their high accuracy, availability, and low-cost single-chip receivers that can be easily integrated into modern embedded systems. Indoor Positioning Systems consist of a network of devices within a GPS-denied indoor environment used to track humans and objects within multistory buildings, train stations, airports, museums, warehouses, etc. Tracking the location of humans within an indoor environment can help maintain social-distance norms during pandemics and can also be used to monitor human traffic behavior within commercial shopping malls. Indoor navigation systems that assist the visually impaired will be significantly improved with the help of precise location feedback to the user. In a multistory environment, indoor positioning systems can be deployed to coordinate fire and rescue operations. These systems can be deployed within a household environment to locate items such as key-fobs and smartphones and can also be used to locate and create path planning layouts for automated robots within warehouses. In contrast with Global Positioning Systems, indoor positioning systems have not achieved the same level of position accuracy. Semiconductor manufacturers have recently released low-cost Ultra-Wideband (UWB) radio transceiver modules capable of centimeter-level distance accuracy and immunity against multipath effects due to their very fine timing resolution. Thus UWB modules can now be

used to develop highly accurate indoor localization systems. In order to determine the location of a mobile tag node within an indoor environment, the locations of the fixed anchor nodes and the anchor-tag distances must be known. This thesis aims to build a scalable self-calibrating anchor scheme that can precisely locate objects in an indoor environment using UWB technology to avoid having to physically measure the location of each anchor node.

1.1 Contributions

The main contributions of this thesis are as follows:

- We propose the Triangle Reconsturction Algorithm (TRA), an anchor self-calibrating algorithm that reduces the number of failures to determine robust quadrilaterals within a network and hence produces an improved location accuracy and Node Localization Success Rate.

- The Triangle Reconstruction Algorithm (TRA) reduces the number of robust quadrilateral "searches" required to localize nodes. Noisy scenarios where nodes are a part of only a single robust quadrilateral will recover from a potential triangle inequality test failure thereby increasing the Node Localization Success Rate.

- We propose Channel Impulse Response Positioning (CIRPos), an anchor self-calibrating algorithm that further builds upon the Triangle Reconstruction Algorithm which analyses the Channel Impulse Response(CIR) metrics to determine the likelihood of whether the UWB distance measurements are made in a NLOS scenario and improves the localization success rate of orphan nodes within the network. CIRPos ensures that there is significant resilience to noisy measurements made as result of NLOS scenarios when attempting to localize orphan nodes.

- CIRPos helps to reduce the amount of unutilized hardware in the network and helps improve the localization capability of the system in scenarios where a tag's ranging capability is limited due to power constraints.

1.2 Document Structure

The document structure is outlined below:

- Chapter 2 covers the background material which includes fundamental concepts of positioning systems, and discusses Ultra-Wideband, existing implementations of network localization and concepts related to graph localizability.
- Chapter 3 describes the novel anchor self-calibrating algorithms: Triangle Reconstruction Algorithm and CIRPos.
- Chapter 4 describes the UWB hardware implementation test setups and the steps taken to reduce ranging error, create an inter-node distance matrix and detect the likelihood of NLOS measurements using Channel Impulse Response metrics .
- Chapter 5 discusses the evaluation metric and the results of our simulations.
- Chapter 6 discusses the conclusion for this thesis.

Chapter 2

Background

2.1 Fundamentals of Positioning Systems

In the following section, we will explore basic radio propagation principles and position determination strategies:

2.1.1 Received Signal Strength Indicator

In this method, we measure the received signal power level at the receiver. The transmitter power level is known, and based on the propagation loss due to signal attenuation, we can calculate the distance between the receiver and transmitter. The free space power at receiver antenna separated by a distance d from the transmitter antenna is given by Friis equation[8]:

$$P_r(d) = \frac{P_t G_t G_r \lambda^2}{(4\pi)^2 d^2 L} \tag{2.1}$$

Where P_t is the transmitted power, $P_r(d)$ is the received power, G_t and G_r are the transmitter and receiver antenna gains, respectively, d is the distance between the transmitter and receiver in meters, and L is a system loss factor, i.e. losses due to transmission line loss, filter loss and antenna loss and alpha is the wavelength in meters. The propagation loss in an indoor environment is not predictable and is hence modeled as a log-normally distributed random variable as shown in [9]:

$$P_r(d) = P_r(d_0) - 10n \log_{10} \left(\frac{d}{d_0} \right) + X_\sigma \tag{2.2}$$

Where d and d_0 are the real and reference distances respectively, $P_r(d)$ is the received signal power at a real distance, $P_r(d_0)$ is the received signal power at reference distance, X is the noise incurred by time-variant sources, and n is the path loss exponent. The loss model is then simplified as [9]:

$$RSSI(d) = A - 10nlog(d) \tag{2.3}$$

Where $RSSI(d)$ is the received signal power at distance d, A is the received signal power at a distance of 1m. The value of n changes according to the environment in which the transmitter and receiver are placed. Orientation of the antennas of the receiver and transmitter can affect the RSSI distance measurement. Using the RSSI method, the signal propagation loss makes it extremely difficult to estimate accurate distances in Non-Line of Sight (NLOS) scenarios.

2.1.2 Angle-of-Arrival (AoA)

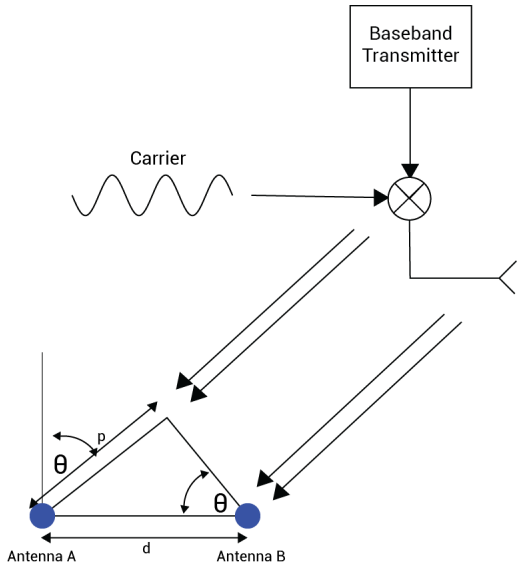

Figure 2.1: Angle of Arrival. Reproduced from [1].

Angle-of-Arrival (AoA) is the method used in position determination to estimate the angle at which the received signal is sent from. Phase Difference of Arrival (PDoA) is the difference between the phases of the receiver carrier signal and is used to calculate the Angle-of-Arrival [1]. In order to calculate the PDoA, two synchronized receivers and a single transmitter are needed, as shown in the image below:

The Path Length p can be calculated by;

$$p = d\sin(\theta) \tag{2.4}$$

where d is the distance between the two antennas and θ is the Angle-of-Arrival. The PDoA is calculated by:

$$\alpha = \frac{2\pi}{\lambda}p = \frac{f}{c}p \tag{2.5}$$

where the signal wavelength is $\lambda = 2\pi c/f$, f is the carrier frequency and c is the speed of light. We can solve Equation 2.4 and Equation 2.5 to find the Angle-of-Arrival:

$$\theta = arcsin\frac{\alpha\lambda}{2\pi d} \tag{2.6}$$

AoA coupled with the inter-node distance measurements is a reliable way of geometric reconstruction of the network layout. AoA based methods need twice the number of receiver modules, thereby increasing the total cost of the network. Some commercially available UWB PDoA kits are limited to the measuring angles only in the front hemisphere of the antenna array. The Bluetooth 5.1 specification introduced the ability to calculate AoA between Bluetooth devices in a 2D plane. It was determined that the Bluetooth 5.1 angle detection functionality has a restricted range and cannot be used to achieve centimeter-level accuracy during localization [10].

2.1.3 Single-Sided Two-Way Ranging (SS-TWR)

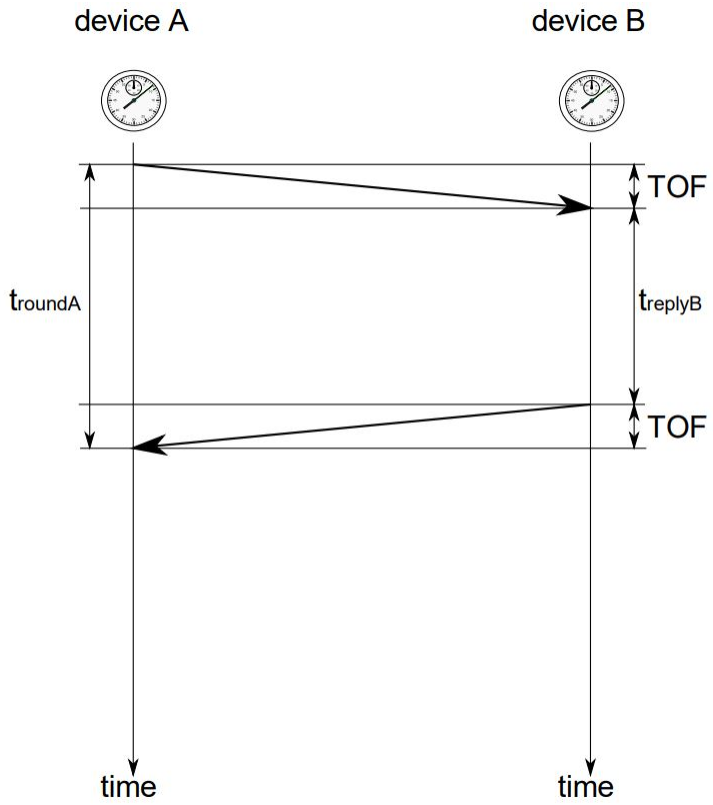

Figure 2.2: Single-Sided Two-Way Ranging scheme [2].

In a two-way ranging scheme, one node acts as an initiator and the other as a responder. The initiator sends a message packet to the responder and records the time t_1 at which the message was transmitted. The responder receives the message and, after some additional processing time t_{reply}, it will send the message back to the initiator. The initiator will receive the packet once again and record the time of reception t_2.

The times recorded by the initiator can be used to calculate the total round trip time taken to exchange the two-ranging message as well as the Time of Flight (ToF):

$$ToF = \frac{(t_1 - t_2 - t_{reply})}{2} \tag{2.7}$$

Assuming the speed of light c is the same as the speed of UWB waves, we can

calculate the distance between the two nodes:

$$Distance = c \times \frac{(t_1 - t_2 - t_{reply})}{2} \tag{2.8}$$

The absolute value of *treply* is dependent on the microcontroller used to control the responder radio module. In practice, two-way ranging using Ultra-Wideband suffers from errors caused by the clock drift of the responder, thus affecting the value of *treply* significantly. In addition to clock drift, the errors in the recorded timestamp are dependent upon the received signal level and hence require additional range bias correction to mitigate such ranging errors [2].

2.1.4 Hyperbolic Trilateration

Hyperbolic Trilateration is the process of calculating the unknown coordinates of a Tag node based on the inter-node distances between the tag and three anchors, as well as the known coordinates of the three anchors, as shown in Figure 2.3. Anchor A determines that the position of the tag lies on the circle created by its radius $r1$ i.e., the inter-node distance between anchor A and the tag. The potential position estimate is further reduced to two different points located at the intersection points of the circles created by Anchor A and Anchor B having radius $r1$ and $r2$, respectively. Finally, the tag's position is reduced to a single point located at the intersection of the three circles created by anchors A, B, and C.

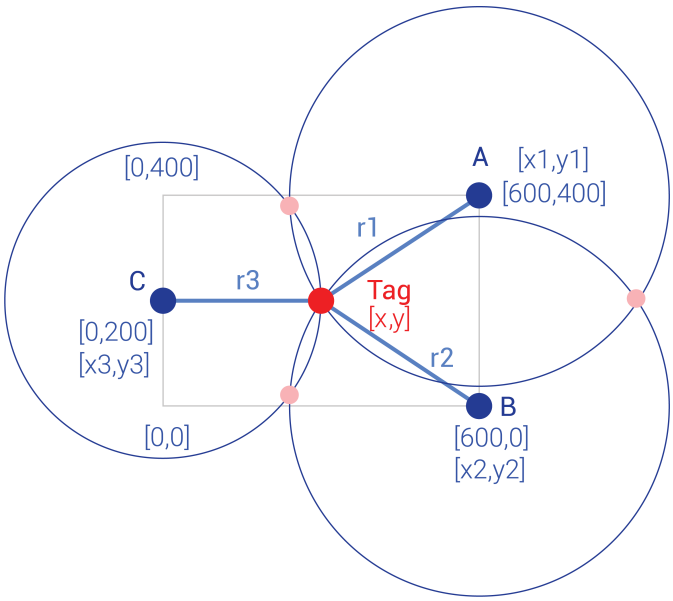

Figure 2.3: An example of Hyperbolic Trilateration.

The inter-node distances between the tag and the three anchors can be calculated using Time-of-Flight (ToF) measurements. The radius of the three intersecting circles gives us three equations:

$$(x - x_1)^2 + (y - y_1)^2 = r_1^2 \tag{2.9}$$

$$(x - x_2)^2 + (y - y_2)^2 = r_2^2 \tag{2.10}$$

$$(x - x_3)^2 + (y - y_3)^2 = r_3^2 \tag{2.11}$$

When expanded, these equations can be solved to produce two new equations:

$$(-2x_1 + 2x_2)x + (-2y_1 + 2y_2)y = r_1^2 - r_2^2 - x_1^2 + x_2^2 - y_1^2 + y_2^2 \tag{2.12}$$

$$(-2x_2 + 2x_3)x + (-2y_2 + 2y_3)y = r_2^2 - r_3^2 - x_2^2 + x_3^2 - y_2^2 + y_3^2 \tag{2.13}$$

The equations are of the form:

$$Ax + By = C \tag{2.14}$$

$$Dx + Ey = F \tag{2.15}$$

The above equations can be linearly solved to produce the (x, y) coordinates of the tag node.

2.2 Ultra-WideBand (UWB)

Ultra-WideBand (UWB) is a wireless technology that can access the frequency spectrum larger than 500MHz [11]. Unlicensed UWB usage in the US has been restricted to operate between 3.1GHz-6GHz at a very low power level below 41.3 dBm/MHz. UWB generates signals of band-limited pulses with an extremely fine resolution such that the receiver can be able to distinguish between multiple reflections of the signal. The IEEE 802.15.4a standard describes the physical layer of the UWB specification added to the original 802.15.4 standard and has defined several channels with a bandwidth of 500MHz.

Heisenberg's uncertainty principle allows us to determine the width of a pulse $\triangle t$ given the bandwidth $\triangle f$ [12]:

$$\triangle f \triangle t \geq 1/4\pi \tag{2.16}$$

The width of the pulse is inversely proportional to the bandwidth, and hence for a very fine timing resolution, we need a large bandwidth. Consider a WiFi system having a bandwidth of 20MHz its pulse timing will be greater than 4ns. From this, we can calculate the pulse length to be 1.2m which gives us a very low-ranging accuracy. Obstructions within an indoor environment can cause the reflected pulse to overlap

the Line of Sight (LOS) pulse, making it hard to detect first path pulse and peak pulse values. On the other hand, the pulse period for UWB signals is approximately 0.16ns wide, which helps to differentiate reflections and estimate the likelihood of whether a signal is of a LOS or a Non Line of Sight (NLOS) type. The fine timing resolution allows the receiver to estimate the Channel Impulse Response (CIR) and accurately detect the first path, peak path, and subsequent reflections.

Detecting the correct first path, peak path amplitude, and sample index values enables accurate ranging measurements between two UWB transceivers.

2.3 Existing Network Localization Techniques

2.3.1 Shape Constraint-based Localization

Convex Position Estimation [13] estimates the locations of nodes within a wireless sensor network based on proximity constraints and antenna radiation patterns. This approach assumes that RF nodes within the network have rotationally symmetric communication ranges, thus creating a radial constraint. Angular constraints such Angle-of-Attack (AoA) is calculated by rotating the receiver node antenna until the maximum receiver signal power level is achieved. Angular constraints are geometrically interpreted as triangles. The intersection of geometric interpretations of the radial constraint and angular constraint estimates the area in which a node may lie. This method relies heavily on the radio antenna's physical characteristics such as orientation and radiation pattern and is also affected by signal attenuation caused due to enclosures, metal, and walls. In [14] the positions of four anchor nodes are estimated with the help of an additional mobile node. The self-calibration algorithm requires the four anchor nodes to be placed in a rectangular shape such that the mobile anchor node lies within the rectangle. In randomly distributed large sensor networks, it is unlikely that the nodes only form rectangular shapes. The self-calibrating algorithm

will also have to be recomputed after placing a mobile node in each of the rectangles formed by the sensor network. Bulusu et al. describe a system that localizes unknown nodes based on the centroid of all anchors in its radio range but their simulations show a localization error of 12% and require 12 anchor nodes per unknown node [15].

2.3.2 Ad-Hoc Localization Systems

Ad-Hoc Localization Systems [16] use the process of iterative multilateration wherein nodes with unknown locations will estimate their positions based on the known location of three fixed nodes. Once its position is estimated, it will add to the list of nodes with known locations, and the process continues until all the unknown nodes are located. Due to the random distribution of the nodes in the network, unknown nodes may not always lie within the range of three neighboring known nodes and hence use multiple hops in order to estimate their position in a process known as Collaborative Multilateration. This method suffers from error accumulation in the position results of unknown nodes. In order to reduce the error accumulation, the total number of nodes with known locations within the network will need to be increased. Savarese et al. describe an iterative approach of selecting a node and assigning coordinates to three of its neighbors based on inter-node distances which results in a localization error of 60% for a ranging error of 5% [17].

In Linear Least Square Estimation (LSE) [18], the nodes in the network can be localized by first initializing the positions of three anchors in order to specify the global translation, global rotation, and global reflection. p_0, p_1 and p_2 represent the node locations of the first three localized anchors in the network. Node p_0 sets the position of the origin; node p_1 sets the first neighbor on the X-axis, and node p_2 sets the Y-axis. The remaining nodes in the system are subsequently trilaterated using the position data of the first three nodes. This algorithm also suffers from error propagation.

$$p_0 := (0, 0) \tag{2.17}$$

$$p_1 := (d_{ab}, 0) \tag{2.18}$$

$$\alpha := \frac{d_{ab}^2 + d_{ac}^2 - d_{bc}^2}{2d_{ab}2d_{ac}} \tag{2.19}$$

$$p2 := (d_{ac}\alpha, d_{ac}\sqrt{1-\alpha^2}) \tag{2.20}$$

2.3.3 DV Hop Algorithm

In the DV-Hop algorithm [19], distance information between anchors and unknown nodes is not shared. One-hop distance data between the anchors in the network are known, and this is used to calculate the average multi-hop distance for each anchor. The product of the number of hops to the nearest anchor node (shortest path) and the average multi-hop distance of that anchor node is used to calculate the position of the unknown node.

$$c_i = \frac{\sum \sqrt{(X_i - X_j)^2 + (Y_i - Y_j)^2}}{\sum_{h_i}} \tag{2.21}$$

where c_i is the Average hop distance and h_i is the hop count between the node and each anchor.

The drawback of such a method is that if an unknown node is within one-hop of its nearest anchor node and the average multi-hop distance of that anchor node is high, then the estimated position of the unknown node will have a large error.

2.3.4 Camera based Approach

In [20] Stereo cameras placed at a fixed distance r can detect the shift disparity d of the objects between the images produced by both cameras. As the focal length f of both cameras is known, the distance D between the lens and the object can be calculated:

$$D = \frac{rf}{d} \tag{2.22}$$

Additional fixed stereo cameras can be placed within an indoor environment to determine the distance to the object from multiple locations. The distance values can then be stitched to calculate the 2D location of the object within the indoor environment. This method can be used to determine the anchor locations but requires several stereo cameras for indoor environments with multiple obstructions thereby increasing the total cost of the system.

2.3.5 Mobile Robot based Algorithm

In the Simultaneous Calibration and Navigation (SCAN) [21] method, a mobile robot is used to generate a map of all the nodes in the sensor network. The algorithm requires a few anchor nodes with known positions placed at strategic locations within the indoor environment. The mobile robot uses odometry and navigation algorithms to estimate its 2D position in the indoor environment. The mobile robot then calculates the positions of the unknown anchor nodes using its own 2D position, orientation, and distance from the unknown anchor using ultrasonic distance measurements. This method is limited by the calibration of the odometry system of the robot and requires the area within the indoor environment to be flat. Any rearrangement of the anchor nodes will require the robot to traverse the network again to find the anchor nodes' new positions.

2.3.6 Multidimensional Scaling (MDS)

The Classical Multidimensional Scaling (MDS) [22] method creates an inter-node Euclidean Distance Matrix with the value zero for node pairs that exceed the ranging limit. Singular Value Decomposition is then performed on the Euclidean Distance Matrix to calculate the locations of each anchor node in the system. Although the

Multidimensional Scaling method can localize all the anchors within the network, it suffers from flip and flex ambiguities resulting in highly inaccurate position estimates.

2.4 Localizability

2.4.1 Graph Rigidity

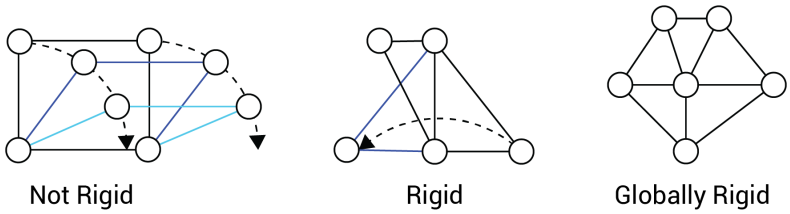

Figure 2.4: Examples of Graph Rigidity. Non-Rigid graphs have infinite realizations. Rigid graphs have a finite number of realizations. Globally rigid graphs have a single realization upto global rotation, translation and reflection. Reproduced from [3].

In a graph realization problem, we assign the nodes within a graph a position based on the Euclidean distance between any adjacent nodes. Saxe [23] concludes that embedding an edge-weighted graph into Euclidean k-space where k=1 is an NP-hard problem. The node locations within a graph are uniquely solvable only if the corresponding graph is generically globally rigid [24]. Laman's Theorem [25] states that a 2D graph G with edges m and vertices n is only generically rigid if each subgraph G' with edges m' and vertices n' satisfies the following equation:

$$m' <= 2n' - 3 \tag{2.23}$$

Hendrickson [26] states that graphs with many edges are more likely to be rigid than those with only a few since the edges are constraining the possible movement of the vertices and also defines an edge of a graph to be infinitesimally redundant if the graph remaining after its removal is infinitesimally rigid i.e. a graph that is not redundantly rigid, will become flexible if any single edge is removed. For example, a triangle

has one realization until it becomes flexible once an edge is removed. Hence graphs that are redundantly rigid do not suffer from flex ambiguities. On the other hand, non-rigid graphs are flexible and can have infinite realizations. However, rigid graphs have two types of disambiguates preventing unique realization, namely flip ambiguity and discontinuous flex ambiguity. In Euclidean-distance based graph realization problems, flex and flip ambiguities can occur due to noisy distance measurements.

2.4.2 Flex Ambiguity

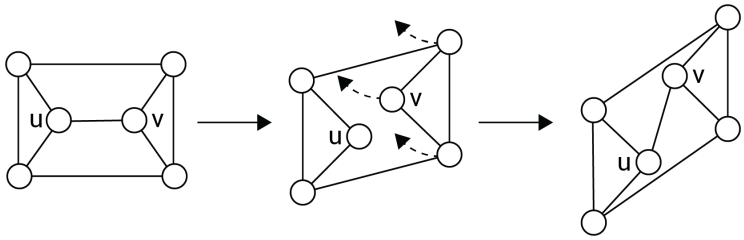

Figure 2.5: Example of Flex Ambiguity. The graph is deformed by the removal of the edge connecting nodes u and v. The edge can still be inserted back between its original vertices. Reproduced from [4].

Discontinuous flex ambiguity occurs when a graph can be deformed by removing an edge to produce a completely different realization, but the removed edge with the same length can still be inserted back between its original vertices [4].

2.4.3 Flip Ambiguity

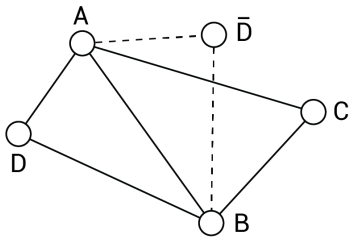

Figure 2.6: Example of Flip Ambiguity. Flip ambiguity in a graph that is rigid but not globally rigid. $\bar{D}$ can be reflected across the edge AB. Reproduced from [5].

When a set of reference nodes are almost collinear, there is a probability that an unknown node can be reflected by a mirror formed from the reference nodes. The reflection process will cause a large localization error, which is the flip ambiguity of node localization [27].

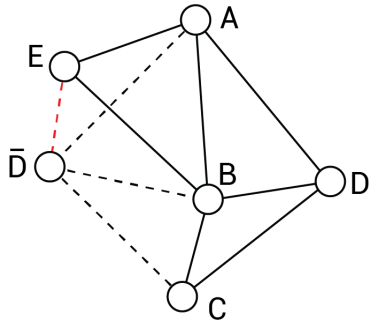

Figure 2.7: Constraining Flip Ambiguity using a verification node. Nodes A, B and C have known positions, node D may experience flip ambiguity and node E is the verification node. Reproduced from [5].

Liu et al. [28] describe how topological constraints can be used to eliminate flip ambiguity with the help of verification nodes. Verification nodes are extra nodes placed at known locations with a limited communication radius R and are not allowed to communicate with other unlocalized unknown nodes. In Figure 2.7, A, B, and C are reference nodes with known positions, E is a verification node, and D and $\bar{D}$ represent the flip positions of the unknown node. During the graph realization process, assume the calculated distance between nodes E and D is $\bar{d_{ED}}$ and it satisfies:

$$\bar{d_{ED}} \leq R \tag{2.24}$$

Since the above equation is satisfied, nodes E and D can communicate with each other which contradicts the communication rules for the verification node E and the position of node D' is excluded from the realization. This method of eliminating flip ambiguity requires several nodes that act as verification nodes and are not used to calculate the Euclidean coordinates of the unknown nodes.

Chapter 3

Methodology

3.1 Robust Quadrilaterals

The Robust Quadrilateral [29] algorithm was implemented to bound the error caused due to noisy measurements and reduce location ambiguity caused due to flip ambiguity and discontinuous flex ambiguity. In this thesis, we propose two novel algorithms Triangle Reconstruction Algorithm (TRA) and Channel Impulse Response Positioning (CIRPos) based on the Robust Quadrilateral algorithm that further improves the sensor network's accuracy and Node Localization Success Rate (NLSR).

Consider a fully-connected 4-node quadrilateral with 6 edges that include the diagonal elements. If we remove a single edge from the graph, we are left with a subgraph containing 4 nodes and 5 edges. The subgraph satisfies Laman's Theorem on rigidity. Since both the quadrilateral and its subgraph satisfy Laman's Theorem, we can conclude that the quadrilateral is redundantly rigid. Since the fully-connected quadrilateral is redundantly rigid, it does not experience discontinuous flex ambiguity. The fully-connected quadrilateral is the simplest geometric shape that is considered redundantly rigid and hence is preferred over other shapes in order to reduce the computational complexity of the graph realization algorithm.

Noisy measurements can cause flip ambiguity even in rigid graphs that satisfy Laman's theorem. The robust quadrilateral algorithm is divided into two main phases:

Cluster Localization and Cluster Transformation. In the cluster localization step, a one-hop inter-node Euclidean Distance Matrix is formed by each origin node. The algorithm then performs a robustness test on all the quadrilaterals within the cluster. If a quadrilateral passes the robustness test, it is considered to be a Robust Quadrilateral. Only nodes that are a part of a Robust Quadrilateral are localized in the cluster localization step.

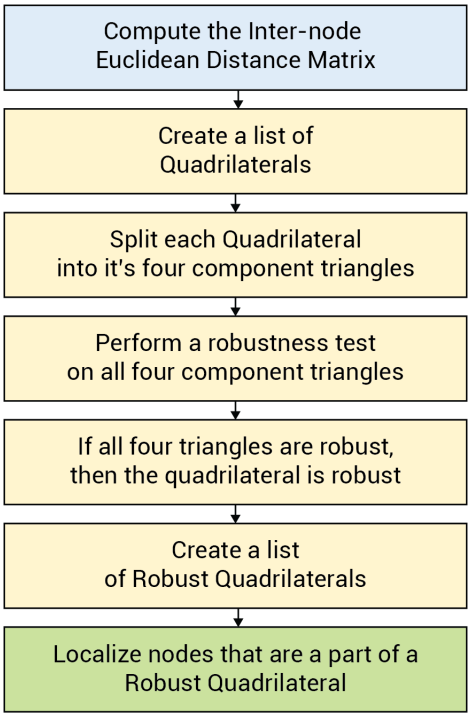

Figure 3.1: Overview of algorithm 1 in the Cluster Localization step of the Robust Quadrilateral Algorithm.

Multiple clusters are stitched together in the Cluster Transformation step by finding three common nodes to form the entire graph.

The probability that a flip occurs within a graph is based on the probability that the measured distance of an edge is closer to the incorrect distance than to the correct distance. In order to determine whether a quadrilateral is a Robust Quadrilateral, it is first divided into its four component triangles. We can calculate the smallest angle θ and smallest side b for each triangle from the Euclidean-distance matrix. We then

perform a robustness test for each component triangle where d_{min} is a threshold value selected based on the measurement noise.

$$b \sin^2 \theta > d_{min} \tag{3.1}$$

Moore et al. [29] show that for a sensor network with zero mean Gaussian error, the probability of flip occurring is bounded by d_{min}. If all four triangles pass the robustness test, then the quadrilateral is considered to be a robust quadrilateral. Once a list of robust quadrilaterals is computed, neighboring robust quadrilaterals are localized if they share three common nodes with an already localized robust quadrilateral. This process continues until the maximum number of nodes within the graph is localized. In order to eliminate flip ambiguity, nodes that are not part of a robust quadrilateral will not be localized.

Although the Robust Quadrilateral algorithm realizes a graph that does not exhibit flip or flex ambiguity, it fails to account for noisy measurements that may prevent the algorithm from performing a robustness test on component triangles that do not pass a Triangle Inequality test as discussed in Section 3.2.

3.2 Robust Triangle Reconstruction

In order to perform a robustness test on the quadrilateral, we need to first perform a robustness test on all four of the component triangles of the quadrilateral. To test the robustness of a component triangle, we need to calculate the values of the smallest angle θ and smallest side b based on the inter-node Euclidean distances of the triangle. If the measured euclidean distances of the triangle are noisy, a condition can arise where the three edges of a triangle fail to pass a Triangle Inequality test [30]. Algorithm 1 in [29] does not perform a Triangle Inequality test on any of the component triangles within the quadrilateral. If the triangle fails to pass the Triangle

Inequality test, the values of the smallest angle θ and smallest side b cannot be calculated, and the robust quadrilateral algorithm will not be able to determine the robustness of that quadrilateral.

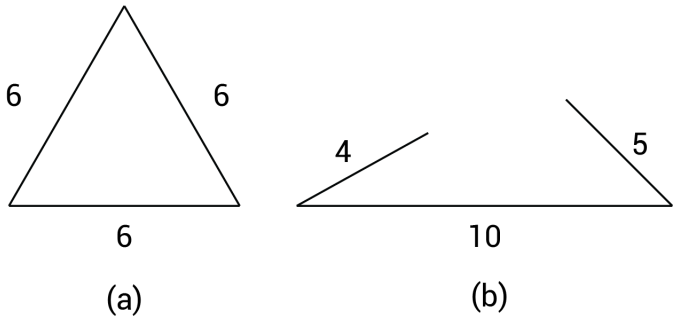

Figure 3.2: (a) A triangle that passes the inequality test. (b) A triangle that fails to pass the inequality test due to noisy measurements.

The Triangle Inequality test states that the sum of any two edges of a triangle is greater than or equal to the third side. For example, a triangle ABC must satisfy all three equations below:

$$A + B > C \tag{3.2}$$

$$A + C > B \tag{3.3}$$

$$B + C > A \tag{3.4}$$

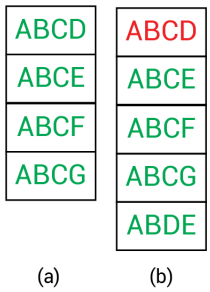

Figure 3.3: Increased number of robust quadrilateral "searches" required to localize the same number of nodes in a network. (a) Only four quadrilaterals need to be tested for their robustness to localize seven nodes. (b) A triangle in quadrilateral ABCD fails the inequality test and hence an additional quadrilateral robustness test is required to localize the same seven nodes. In a noisy environment with a large number of nodes, triangle inequality test failures can significantly increase the computation time.

Figure 3.3 shows a scenario where a robustness test is being performed on all four of the component triangles of a quadrilateral. Let us assume that 3 out 4 of the triangles are determined to be robust. The algorithm now attempts to test the robustness of the fourth triangle but fails to do so since the triangle does not pass the Triangle Inequality test due to a noisy measurement even if the true values of the edges of the triangle would typically pass the Triangle Inequality test. In such a scenario, the unlocalized nodes of that quadrilateral will have to be located based on a different quadrilateral altogether. This will unpredictably increase the total computation time since the algorithm needs to search for additional robust quadrilaterals to localize the same set of nodes.

Consider another scenario where a particular unlocalized node in the graph is part of only a single robust quadrilateral and multiple non-robust quadrilaterals(assuming zero noise). In a noisy environment, the robustness of the quadrilateral cannot be determined (if one of the triangles fails to pass the Inequality test), then that node will remain unlocalized, thereby reducing the Node Localization Success Rate of the entire graph.

The novel algorithm attempts to reconstruct triangles that fail to pass the inequality test with the aim of reducing the number of quadrilateral "searches" required to

localize the nodes in a network and also to increase the Node Localization Success Rate of unlocalized nodes that would have otherwise been localized as part of a robust quadrilateral.

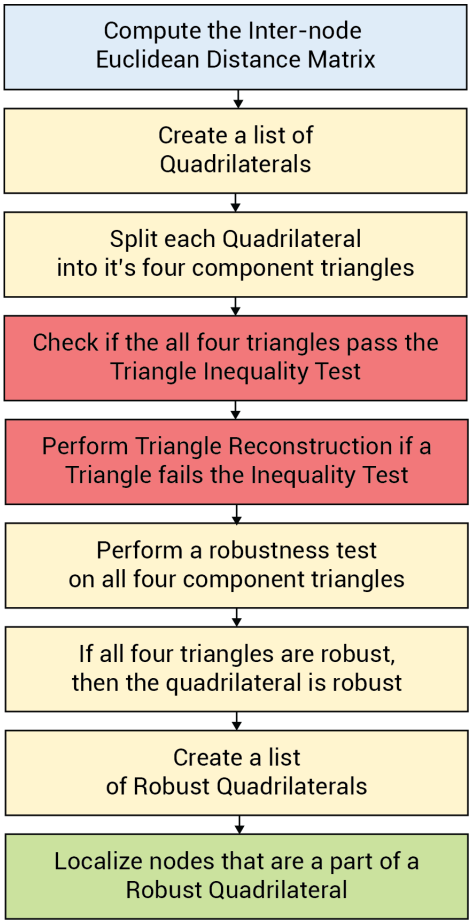

Figure 3.4: Overview of the Triangle Reconstruction Algorithm (TRA).

We use the inter-node Euclidean distances of the quadrilateral to reconstruct the triangle that failed the inequality test. Our novel Triangle Reconstruction Algorithm (TRA) first performs an inequality test on each of the four component triangles of the quadrilateral. If all four triangles pass the inequality test, the robustness of the quadrilateral is determined; else, the number of triangles that fail the inequality test is determined. If the number of triangles that fail the inequality test is greater than 1, then TRA does not classify the quadrilateral to be robust. When a single triangle within the quadrilateral fails the inequality test, we attempt to perform triangle

reconstruction of that triangle and recompute the robustness of the quadrilateral.

The Triangle Reconstruction Algorithm does not use the edge of the triangle (that fails to pass the Inequality test) that also acts as one of the diagonals of the quadrilateral. By doing so, we prevent the reconstruction of a new triangle that will also fail the Inequality test. Instead, we use the two sides, diagonal and the two angles formed by the sides and diagonal of the quadrilateral that are not a part of that triangle. We can then use these values to calculate new dimensions of each side of the triangle using the Law of Cosines [31]:

$$c^2 = a^2 + b^2 - 2ab\cos(C) \tag{3.5}$$

Once the sides of the new triangle are determined, TRA will recalculate the internal angles of the triangle and recompute the robustness tests for the quadrilateral.

3.3 Localizing Orphan Nodes based on Channel Impulse Response (CIR) Metrics

The Robust Quadrilateral algorithm does not localize nodes that are not a part of a robust quadrilateral due to their ability to experience flip ambiguity. These unlocalized nodes are referred to as orphan nodes. Orphan anchor nodes remain unutilized and cannot be used for accurate tag localization, thereby increasing the localization system's cost and energy consumed. Since anchors are usually powered through a mains supply, the total energy consumed by orphan anchor nodes is negligible. However, this is not the case for battery-operated tag nodes that may operate their UWB radios at a lower power level in order to increase their battery life. Consider a scenario where a tag that is operating its UWB radio at a lower power level has a reduced ranging capability. Assuming the tag's ranging capability is limited to only two robust anchor nodes and one orphan anchor node. In this scenario, it is not possible

to accurately estimate the tag's location within the indoor environment. Hence, it is important to find a solution capable of estimating the locations of orphan nodes without decreasing the system's overall accuracy.

Line-of-Sight (LOS) distance measurement errors usually occur due to clock drift and received signal level that can be minimized as described in section TWR Error Calibration. Non-Line-of-Sight (NLOS) distance measurements usually occur due to multipath reflections caused by obstructions that can result in a large error. Our novel algorithm makes use of the UWB receiver's Channel Impulse Response (CIR) metrics to determine the probability that a distance measurement was made in a LOS or NLOS situation. The probability that a distance measurement was made in a NLOS situation is referred to as Confidence Level (CL). Section 4.3 describes the process of calculating the Confidence Level.

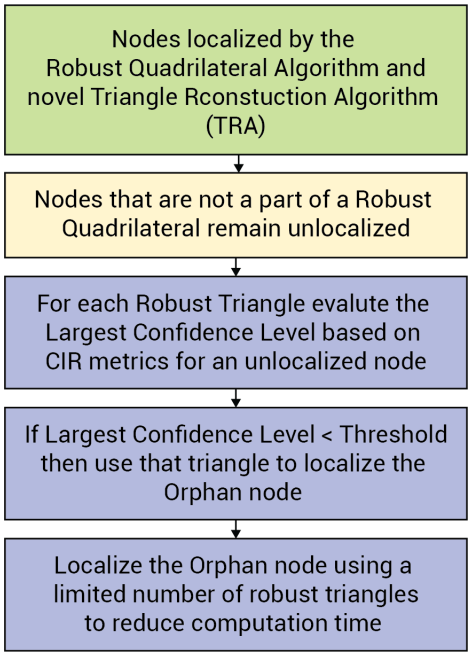

Figure 3.5: Overview of the novel CIRPos algorithm.

For each distance measurement made in the inter-anchor node Euclidean distance matrix, a corresponding Confidence Level is assigned to it. Predetermining the placement of an anchor node within the indoor environment cannot always guarantee that

distance measurements made between that node and other nodes are always going to be in LOS situations and free of multipath reflections. Hence in any practical deployment we assume that some of the inter-anchor node distance measurements in the generated Euclidean distance matrix will contain measurements made in NLOS conditions. Our novel algorithm referred to as CIRPos attempts to localize orphan nodes and reduce the effect of NLOS measurements that may have caused a node to be unlocalized after the robust quadrilateral localization process was carried out.

Once the robust quadrilateral process has been completed, CIRPos will find all the robust triangles within the network and will attempt to use them to trilaterate the location of the orphan node. Amongst each of the distance measurements made between the three nodes of the robust triangle and the orphan node, CIRPos calculates the largest Confidence Level. If the largest Confidence Level value is greater than a certain threshold, then that triangle is not used to trilaterate the position of the orphan node. The largest Confidence Level is used to bound the error caused due to NLOS measurements. The threshold value is determined by the system designer based on the indoor environment. For example, an indoor floor plan without a large number of walls or obstructions can have a lower threshold value. The position of the orphaned node is overfitted by using all the available robust triangles within the network. A limit can be placed on the total number of robust triangles used to locate the orphan node in order to reduce the computation time.

Chapter 4

Implementation

4.1 Minimizing Two-Way Ranging Error

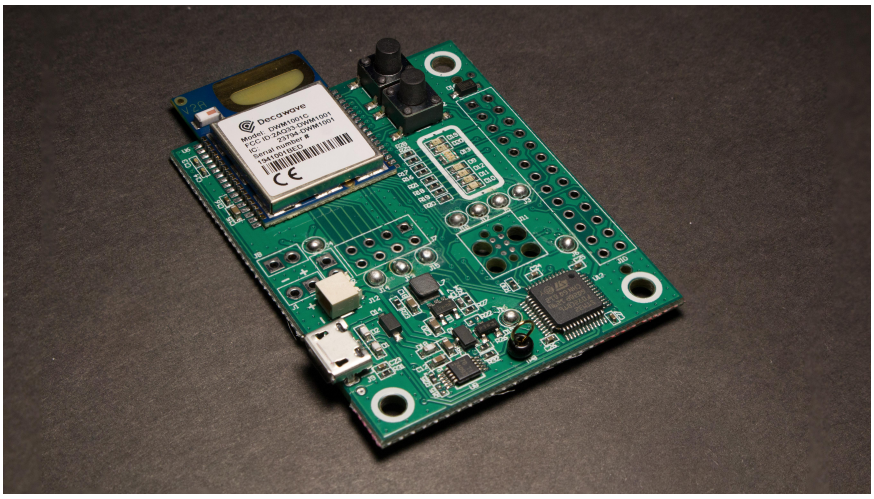

Figure 4.1: Decawave DWM1001 UWB Development Board

The Decawave DWM1001 UWB development board is used to measure inter-node distances and provide an estimation of the ranging accuracy at various distances. It contains the DW1000 UWB radio transceiver and an nRF52833 System-on-Chip (SoC) to control it. Decawave states that an uncalibrated DW1000-based board can achieve a minimum standard deviation of 30cm, and for a DW1000-based board that is calibrated for antenna delays, it can achieve a minimum standard deviation of 4.5cm for 2000 measurements.

4.1.1 Calibrating Antenna Delays

In a two-way ranging scheme between two nodes A and B, as shown in Figure 2.2, the dominant error in ranging accuracy is caused by [2]:

$$Error = \frac{1}{2} t_{replyB}(e_a - e_b) \tag{4.1}$$

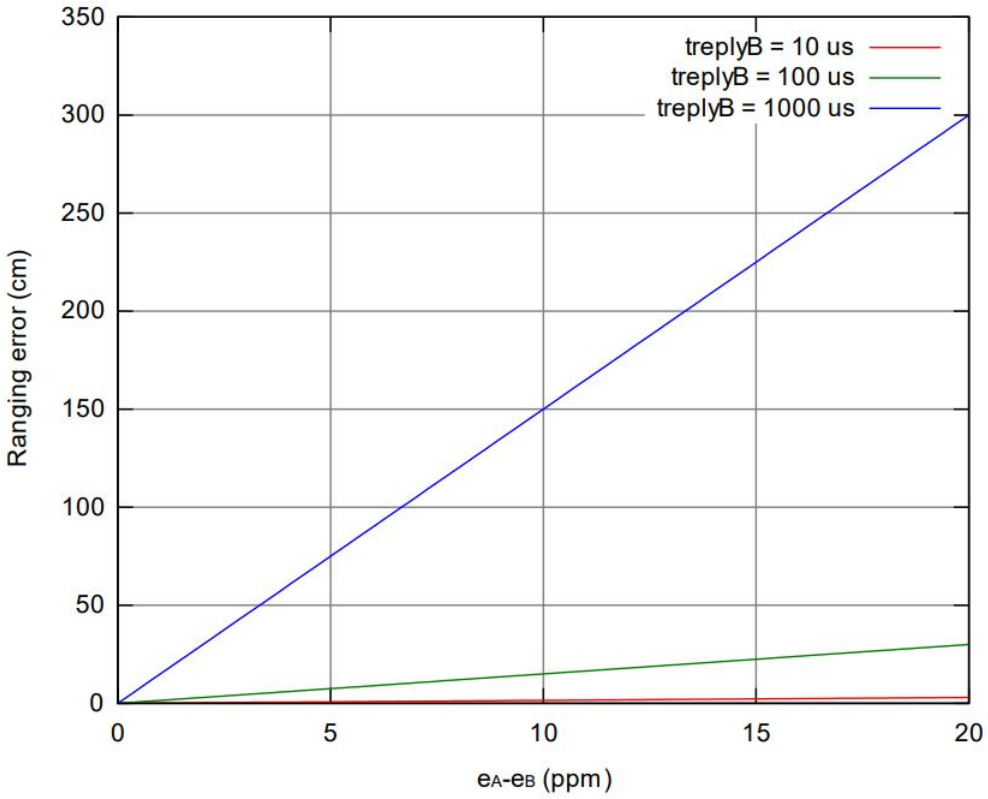

Figure 4.2: Ranging Error in a TWR scheme [2].

Figure 4.2 shows that the error is strongly dependent upon t_{replyB}. The value of t_{replyB} is associated with the propagation delay from when the transmitter timestamps are applied to the points at which the receiver's message has been captured [2]. These delays are inherent to the radio transceiver chip and are referred to as transmitter and receiver antenna delays. The total measured time that is used to calculate the Time of Flight (ToF) value should include the antenna delays for the transmitter and

receiver:

$$t_{Measured} = t_{ADTX} + ToF + t_{ADRX} \tag{4.2}$$

Where $t_{Measured}$ is the measured time from the transit timestamp to the receiver timestamp, t_{ADTX} is the transmitter antenna delay, and t_{ADRX} is the receiver antenna delay. Hence, in order to accurately determine the distance between two nodes, it is extremely important to properly calibrate the antenna delays of the DWM1001 board.

To calibrate the antenna delay of a DWM1001 board, we need a reference device that has already had its antenna delay calibrated. Section 4.2 describes the process needed to create a reference device. Once we have created a reference device, we can use it to perform distance measurements with the DWM1001 board that is under test. Both the boards are placed at a recommended calibration distance depending upon the channel number and Pulse Repetition Frequency (PRF), as shown in Table 4.1.

Channel Number	**PRF (MHz)**	**Distance (m)**
2	16	12.9
2	64	8.1
3	16	11.5
3	64	7.2
4	16/64	8.7
5	16	7.9
5	64	5
7	16/64	5.3

Table 4.1: Calibration distance for channels and PRF [2].

Once the boards are separated by the recommended calibration distance, the

antenna delay values for both the transmitter and receiver can be manually adjusted within the transmitter SS-TWR code until the ranging error is minimized. The antenna delay for the Device Under Test (DUT) is initially set to 515ns, and 1000 TWR measurements are carried out before any adjustment is made to the antenna delay value. In our test setup, we placed two DWM1001 boards in a LOS scenario at a calibration distance of 5m since the channel number was set to 5, f_c was at 6.5GHz, and the PRF was set to 64MHz. It was observed that the error was minimized to -11cm when the transmitter antenna delay was set to 16.30ns and the receiver antenna delay was set to 16.453ns.

4.1.2 Range Bias Correction based on Received Signal Level(RSL)

In our SS-TWR test setup, we minimized the observed ranging error between two DWM1001 boards to -11cm by calibrating the antenna delays. It was observed that as we move away from the recommended calibration distance of 5m, the ranging error changes in magnitude and polarity depending upon the direction in which the boards are moved with respect to each other. The range of error was observed to be between 8.37 cm and -26.41cm as the distance between two boards varied between 50cm and 1000cm.

In an ideal scenario, there is no relationship between the reported timestamp of a received signal and the Received Signal Level(RSL)[2]. However, in practice, the measured timestamp, when compared to the correct value, produces a bias in the timestamp that is related to the RSL value. This time bias can be converted to a range bias, and the effect of RSL on range bias is shown in Figure 4.3.

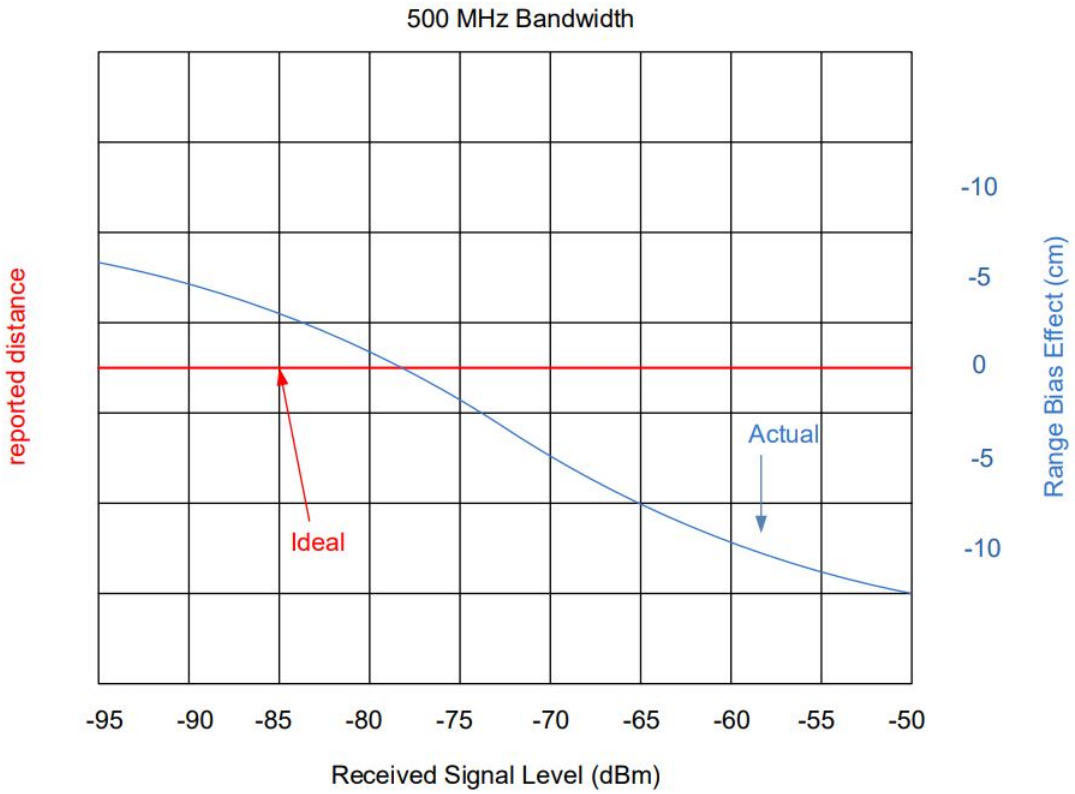

Figure 4.3: The ideal and actual effect of range bias on the reported distance [2].

The measured distance can be corrected such that:

$$\text{Actual Distance} = \text{Measured Distance - Range Bias Correction Factor} \tag{4.3}$$

The 4.2 shows the relationship between RSL and the range bias correction factor for Decawave DW1000 based boards. In our test setup, we set the channel to 5, PRF to 64MHz, and our "zero-point" was calibrated at 5m which relates to the RSL value of -77dBm.

RSL (dBm)	PRF 64MHz (cm)
-61	-11
-63	-10.5
-65	-10
-67	-9.3
-69	-8.2
-71	-6.9
-73	-5.1
-75	-2.7
-77	0
-79	2.1
-81	3.5
-83	4.2
-85	4.9
-87	6.2
-89	7.1
-91	7.6
-93	8.1

Table 4.2: Relationship between Received Signal Level and Range Bias correction factor for DW1000-based boards [2].

We can estimate the RSL in dBm using the equation [32]:

$$\text{RX Level} = 10 \times \log_{10}\left(\frac{C \times 2^{17}}{N^2}\right) - A \text{ dBm} \tag{4.4}$$

Where C is the Channel Impulse Response Power, A is a constant 121.74 for a PRF of 64MHz and N is the Preamble Accumulation Count.

In our test setup, we calculated the received signal power level (RX Level) for each

distance measurement made at 50cm increments ranging from 50cm to 1000cm. We extrapolated additional bias correction factor values based on Table 4.2 using linear regression and applied them to the distance measurements in our test setup as shown in Table 5.2.

To further improve the accuracy of the measured distances, in our test setup, we also applied the bias correction factor based on the relationship of measured distance and received signal power as shown in [7].

Range (m)	**RX Power (dBm)**
1	-63
2	-69
3	-72.6
4	-75.1
5	-77
6	-78.6
7	-79.9
8	-81.1
9	-82.1
10	-83
13	-85.3

Table 4.3: Relationship between Received Signal Power and Range [7].

The values in Table 4.3 are recommended by Decawave to improve the performance of DW1000 based systems. The receiver power level in the above table are calculated using Friis' path loss formula configured for a DW1000 system [2]

$$P_R[dBm] = P_T[dBm] + G[dB] + 20\log_{10}(4\pi f_c R) \tag{4.5}$$

Where P_R is the RSL, P_T is the transmitted power and is -14.3dBm for a DW1000, G is the transmitter and receiver gain, which is set to +2dB, c is the speed of light, f_c is the center frequency of the channel, which is 6.5GHz and R is the measured distance between the two nodes.

4.2 Reference Node Generation

In 4.1.1, we calibrated the antenna delay for a single node at a time using a reference device with a known calibration. In this section, we will discuss the procedure to create a reference device.

In order to create a reference device, three DWM1001 boards are arranged in an equilateral triangle layout and the distance between each board is a known value. A Euclidean distance matrix is then generated from the three nodes.

In our custom test setup, we laser cut an equilateral triangle jig having a side length of 80cm that equally spaces and orients the DWM1001 boards towards each other.

After applying the TWR antenna delay calibration reference device generation algorithm described in [33] for our custom jig, the three DWM1001 boards in our test setup have antenna delays: 10.788ns, 10.784ns, and 10.788ns. These devices can now be used as reference devices in order to calibrate the distance for a DUT as described in 4.1.1.

4.3 Calculating Channel Impulse Response (CIR) Metrics

Our novel algorithm CIRPos makes use of Channel Impulse Response (CIR) metrics to estimate the probability that a distance measurement was made in an NLOS scenario.

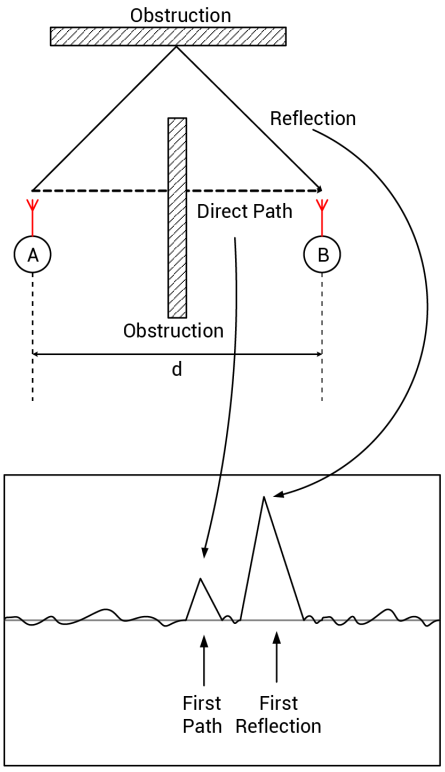

Figure 4.4: A typical NLOS scenario with the expected receiver accumulator results [6].

In Figure 4.4 we can observe what the typical accumulator of the DW1000 looks like in a simple NLOS scenario. The first path has a lower amplitude than the first reflection indicating the direct path has been attenuated by an object, and the reflected path may be used to calculate the ToF measurement instead.

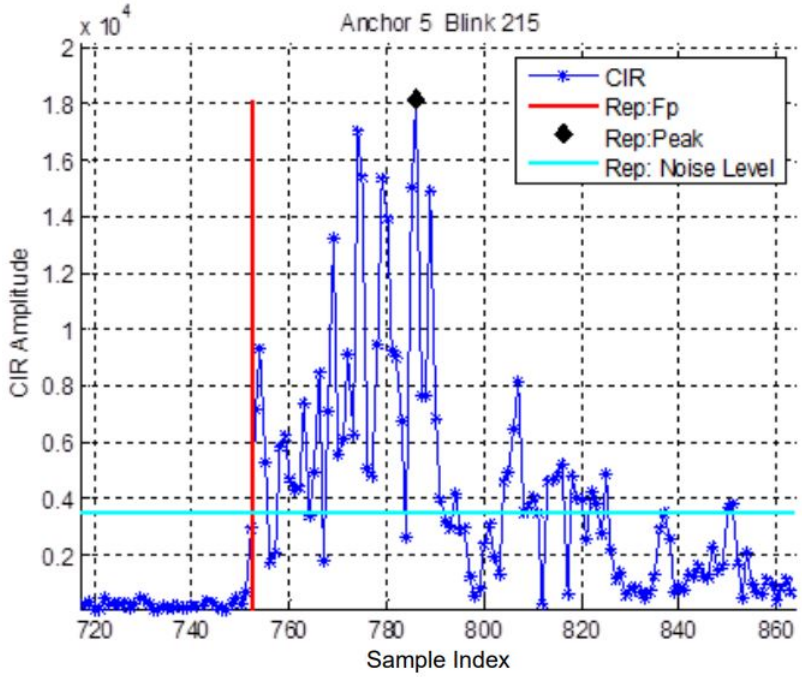

Figure 4.5: A real NLOS scenario with the observed receiver accumulator results [6].

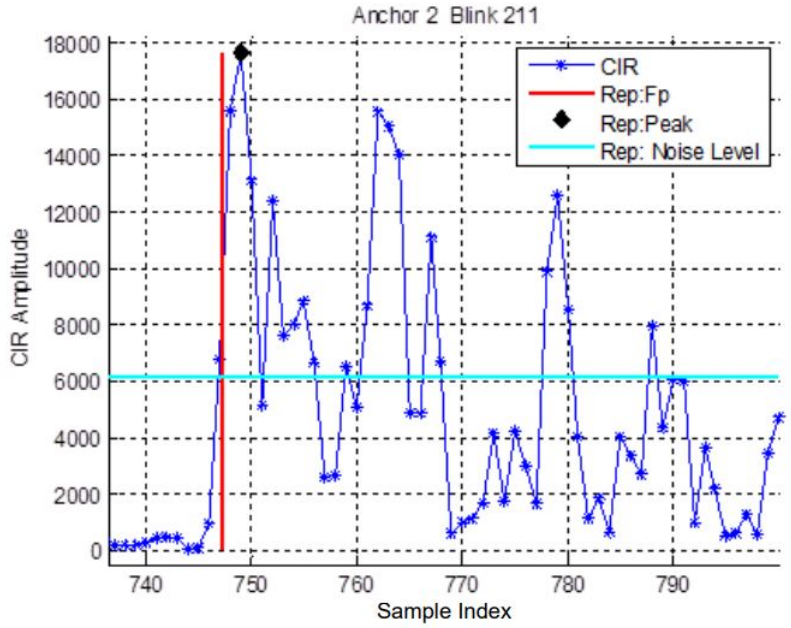

Figure 4.6: A real LOS scenario with the observed receiver accumulator results [6].

Figure 4.5 shows a sample accumulator from a real NLOS scenario. We can observe that the first path amplitude is less than the peak amplitude and lies much further

in front of the peak path position. Figure 5.1 shows a sample accumulator from a real LOS scenario. We can observe that the first path amplitude is still less than the peak amplitude, but it lies much closer to the peak path position.

The first path position and the peak path position can be compared to give the likelihood that the distance measurement is an NLOS measurement. The absolute difference in the two path positions can be further processed to give us a Confidence Level (CL) as shown [6]:

$$ID_{iff} = |\text{ first path position - peak path position }| \tag{4.6}$$

$$CL = \begin{cases} 0, & ID_{iff} \leq 3.3 \\ 0.39178 \times ID_{iff} - 1.31719, & ID_{iff} < 6.0 \text{ and } ID_{iff} > 3.3 \\ 1, & \text{otherwise} \end{cases} \tag{4.7}$$

In our test setup, the DWM1001 boards read the Lead Edge Detection Peak Path Index sub-register to find the position index of the detected peak path in the Channel Impulse Response(CIR) and also read the Receive Time Stamp register in order to find the position index of the first path in the CIR. These register values are then used to calculate the Confidence Level as described in Equation 4.6 and Equation 4.7. In our simulations we associated randomly generated values for Confidence Level with each distance measurement depending upon the input noise level.

4.4 Inter-Node Euclidean Distance Matrix Generation

The Decawave DWM1001 development board includes a DW1000 UWB radio transceiver and an nRF52 SoC, which controls the radio transceiver and also has a Bluetooth 4.2 stack implemented on it. The Positioning and Networking Stack (PANS) is a firmware

abstraction provided by Decawave that allows us to control the radio transceiver; discover, join and leave networks; and also allows us to configure the DWM1001 as an anchor or a tag and uses the 802.15.4 standard to send UWB packets [34] [35].

The PANS library does not provide the ability to send UWB data frames to a particular device based on the Destination Address. Hence we need to find an alternative approach to obtaining all the inter-node distance measurements on a centralized node. In our test setup, we implemented a communication scheme that uses the PANS anchor and tag drivers to create a Euclidean distance matrix on a centralized node and laser cut a jig that places four DWM1001 boards in a square shape having a side length of 80cm.

Chapter 5

Results and Analysis

5.1 Evaluation Criteria

We evaluate the performance of the UWB transceiver's ability to estimate distance measurements accurately in an indoor environment. The Root Mean Square Error σ_d of the distance measurements is expressed as:

$$\sigma_d = \sqrt{\sum_{i=1}^{M} \frac{\left(\bar{d_i} - d_i\right)^2}{M}} \tag{5.1}$$

where $\bar{d_i}$ is the real distance, d_i is the measured distance and M is the total number of measurements. We evaluate the location accuracy of our novel algorithm for different levels of input noise to simulate an indoor environment and compute how the localization differs from the known ground truth. The location error is the Root Mean Square Error σ_p in Euclidean 2D space:

$$\sigma_p = \sqrt{\sum_{i=1}^{N} \frac{\left(\bar{x_i} - x_i\right)^2 + \left(\bar{y_i} - y_i\right)^2}{N}} \tag{5.2}$$

where $\bar{x_i}$ and $\bar{y_i}$ are the real coordinates of the nodes, x_i and y_i are the measured coordinates of the nodes, and N is the total number of anchor nodes in the network. We evaluate the ability of the novel algorithm anchor self-calibrating algorithms TRA

and CIRPos to localize all the anchor nodes within the network successfully. The percentage of successfully localized anchors is known as Node Localization Success Rate (NLSR) and is given by:

$$NLSR = \frac{L \times 100}{N} \tag{5.3}$$

where L is the total number of successfully localized anchor nodes in the system and N is the total number of anchor nodes, including the unlocalized anchor nodes in the system.

Another useful metric is to gauge the computation time required to realize the graph in seconds. In order to minimize the computation time, we recommended that the centralized node that computes the locations of the nodes in the network and is connected to a gateway computer with higher processing speeds than the nRF52 SoC.

5.2 Simulated Deployment

5.2.1 Distance Accuracy

We have tested the ability of the Decawave DWM1001 UWB boards to achieve distance measurements with a high accuracy. We measured the distances between one DWM1001 board calibrated for antenna delays and a reference device as described in Section 4.2. Each reading was an average of 100 TWR measurements at 50cm increments ranging from 50cm-1000cm. Table 5.1 shows the distance measurement error after the antenna delays are calibrated. The distance measurement Root Mean Square Error (RMSE) post antenna delay calibration is 14.13cm. Table 5.2 shows the distance measurement error after the Range Bias Correction is applied based on the calculated Received Signal Level (RSL). The distance measurement Root Mean Square Error (RMSE) post Range Bias Correction is 10.59cm. Table 5.3 shows the

distance measurement error after the Range Bias Correction is applied based on the calculated Measure Distance values as described in [7]. The distance measurement Root Mean Square Error (RMSE) post the recommended distance based correction factor is 6.15cm.

Real Distance (cm)	Measured Distance (cm)	Error (cm)
50	41.625	8.37
100	92.760	7.23
150	146.68	3.31
200	199.75	0.25
250	250.74	-0.74
300	307.11	-7.11
350	356.20	-6.20
400	401.84	-1.84
450	454.58	-4.58
500	511.73	-11.73
550	563.77	-13.77
600	615.33	-15.33
650	663.49	-13.49
700	718.4	-18.4
750	768.45	-18.45
800	816.33	-16.33
850	867.6	-17.6
900	923.2	-23.2
950	972.96	-22.96
1000	1026.4	-26.41
Mean (cm)		**-9.95**
Standard Dev (cm)		**10.38**
RMSE (cm)		**14.13**

Table 5.1: Measured Two-Way Ranging distance error between two UWB transceivers after antenna delay calibration. The separation distance was incremented by 50cm for a range of 50cm-1000cm. At each separation distance, 100 TWR measurements were sampled and averaged.

Real Distance	Measured Distance	FP1	FP2	FP3	CIR	Pream	RX_POWER	RSL Bias Correcton Factor	Distance RSL Bias Corrected	Error
50	41.625	9	6	48	35	52	-89.44	7.1	34.52	15.47
100	92.760	36	63	19	11	52	-94.47	10.6	82.16	17.83
150	146.68	51	50	24	29	52	-90.26	7.8	138.88	11.11
200	199.75	51	32	63	16	52	-92.84	9.25	190.5	9.5
250	250.74	1	33	56	30	52	-90.11	7.8	242.94	7.05
300	307.11	46	12	32	6	52	-97.1	12.72	294.39	5.6
350	356.20	30	46	26	12	52	-94.09	10.64	345.56	4.43
400	401.84	5	53	60	57	52	-87.32	5.77	396.07	3.92
450	454.58	49	34	18	37	52	-89.2	7.16	447.42	2.57
500	511.73	7	53	8	8	52	-95.85	11.33	500.39	-0.39
550	563.77	33	34	52	19	52	-92.09	9.25	554.52	-4.52
600	615.33	5	46	52	17	52	-92.58	9.25	606.08	-6.08
650	663.49	12	34	14	48	52	-88.07	6.47	657.02	-7.02
700	718.4	37	49	45	47	52	-88.16	6.47	711.93	-11.93
750	768.45	34	31	39	58	52	-87.25	5.77	762.68	-12.68
800	816.33	49	0	28	52	52	-87.72	5.77	810.56	-10.56
850	867.6	56	63	0	25	52	-90.9	7.86	859.74	-9.74
900	923.2	4	41	37	39	52	-88.97	6.47	916.73	-16.73
950	972.96	42	46	12	25	52	-90.9	7.86	965.1	-15.1
1000	1026.4	18	36	55	8	52	-95.85	11.33	1015.08	-15.08
Mean (cm)										-1.61
Standard Dev (cm)										10.74
RMSE (cm)										10.59

Table 5.2: Measured Two-Way Ranging distance error between two UWB transceivers after Receiver Signal Level was measured and the appropriate RSL bias correction factor was applied. The separation distance was incremented by 50cm for a range of 50cm-1000cm. At each separation distance, 100 TWR measurements were sampled and averaged.

Real Distance	Measured Distance	RSL Bias Corrected	Friis RSL	Distance Correction Factor	Final Estimated Distance	Error
50	41.625	34.52	-63	-10.5	**45.02**	**4.98**
100	92.760	82.16	-63	-10.5	**92.66**	**7.34**
150	146.68	138.88	-69	-8.2	**147.08**	**2.92**
200	199.75	190.5	-69	-8.2	**198.7**	**1.3**
250	250.74	242.94	-72.6	-5.1	**248.04**	**1.96**
300	307.11	294.39	-72.6	-5.1	**299.49**	**0.51**
350	356.20	345.56	-75.1	-2.7	**348.26**	**1.74**
400	401.84	396.07	-75.1	-2.7	**398.77**	**1.23**
450	454.58	447.42	-77	0	**447.42**	**2.58**
500	511.73	500.39	-78.6	2.1	**498.29**	**1.71**
550	563.77	554.52	-78.6	2.1	**552.42**	**-2.42**
600	615.33	606.08	-79.9	2.8	**603.28**	**-3.28**
650	663.49	657.02	-79.9	2.8	**654.22**	**-4.22**
700	718.4	711.93	-81.1	3.5	**708.43**	**-8.43**
750	768.45	762.68	-81.1	3.5	**759.18**	**-9.18**
800	816.33	810.56	-82.1	3.8	**806.76**	**-6.76**
850	867.6	859.74	-82.1	3.8	**855.94**	**-5.94**
900	923.2	916.73	-83	4.2	**912.53**	**-12.53**
950	972.96	965.1	-83	4.2	**960.9**	**-10.9**
1000	1026.4	1015.08	-85.3	4.9	**1010.18**	**-10.18**
Mean (cm)						**-2.83**
Standard Deviation (cm)						**5.82**
RMSE (cm)						**6.15**

Table 5.3: Measured Two-Way Ranging distance error between two UWB transceivers after the recommended measured distance based bias correction factor was applied. The separation distance was incremented by 50cm for a range of 50cm-1000cm. At each separation distance, 100 TWR measurements were sampled and averaged.

5.2.2 Location Accuracy

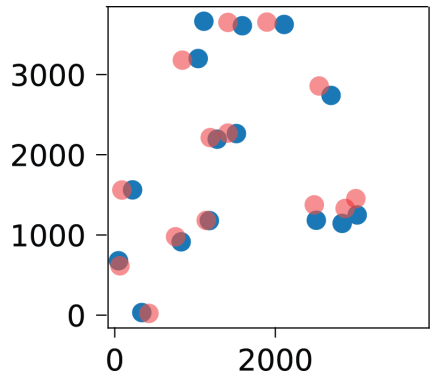

Figure 5.1: Simulation results of CIRPos with TRA. The blue nodes indicate the true locations of the anchor nodes. The red nodes indicate the estimated locations of the anchors nodes which uses CIRPos along-with TRA. The location error is 52.84cm and the NLSR is 93.33% in a simulated environment with input noise having standard deviation of 20cm. The floorplan dimensions is 4000cm x 4000cm and contains 15 nodes.

Input Noise	**Exisiting Algorithms**			**Novel Algorithms**	
σ_d	**LSE**	**MDS**	**RQ**	**TRA**	**CIRPos**
1 cm	5.02 cm	3.41 cm	6.84 cm	5.31 cm	4.98 cm
5 cm	24.90 cm	28.92 cm	16.24 cm	10.87 cm	10.09 cm

Table 5.4: Comparison of Location Error for Anchor Self-Calibrating Schemes in a small area. The location error is calculated in a simulated environment with input noise having standard deviation of 1cm and 5cm. The floorplan dimensions is 200cm x 200cm and contains 15 nodes.

Input Noise	**Exisiting Algorithms**			**Novel Algorithms**	
σ_d	**LSE**	**MDS**	**RQ**	**TRA**	**CIRPos**
20 cm	178.4 cm	198.2 cm	60.5 cm	57.33 cm	54.84 cm

Table 5.5: Comparison of Location Error for Anchor Self-Calibrating Schemes in a large area. The location error is calculated in a simulated environment with input noise having standard deviation of 20cm. The floorplan dimensions is 4000cm x 4000cm and contains 15 nodes.

Table 5.4 and Table 5.5 shows the location error of our novel algorithms TRA and CIRPos in comparison to existing anchor self-calibrating schemes. For a noise level with standard deviation of 1cm, there is no significant improvement. The novel algorithm CIRPos significantly reduces the location error when compared to LSE and MDS for an input noise having standard deviation of 5cm and 20cm.

5.2.3 Node Localization Success Rate (NLSR)

Input Noise	**Existing Algorithms**			**Novel Algorithms**	
σ_d	**LSE**	**MDS**	**RQ**	**TRA**	**CIRPos**
1 cm	100%	100%	85.32%	88%	93.33%
5 cm	100%	100%	50.66%	61.33%	96%

Table 5.6: Comparison of Node Localization Success Rate in a small area. The location error is calculated in a simulated environment with input noise having standard deviation of 1cm and 5cm. The floorplan dimensions is 200cm x 200cm and contains 15 nodes.

Input Noise	**Existing Algorithms**			**Novel Algorithms**	
σ_d	**LSE**	**MDS**	**RQ**	**TRA**	**CIRPos**
20 cm	100%	100%	53.18%	69.26%	91%

Table 5.7: Comparison of Node Localization Success Rate in a large area. The location error is calculated in a simulated environment with input noise having standard deviation of 20cm. The floorplan dimensions is 4000cm x 4000cm and contains 15 nodes.

Table 5.6 and Table 5.7 show the Node Localization Success Rate (NLSR) in a small and large indoor environment. When the input noise is very low, the NLSR of all the algorithms is significantly high and almost all the nodes are localized. As the input noise increases and the dimensions of the indoor environment is expanded, the NLSR for the Robust Quadrilateral decreases. The novel algorithm TRA has an improved NLSR whereas CIRPos has a significant increase in the NLSR when compared to the Robust Quadrilateral algorithm.

5.2.4 Computation Time

Input Noise	Existing Algorithms			Novel Algorithms	
σ_d	**LSE**	**MDS**	**RQ**	**TRA**	**CIRPos**
1 cm	0.1108s	0.003s	3.0379s	2.8632s	4.3254s
5 cm	0.104s	0.0012s	16.444s	16.85s	24.808s

Table 5.8: Comparison of Computation Time for Anchor Self-Calibrating Schemes in a small area. The computation time is calculated in a simulated environment with input noise having standard deviation of 1cm and 5cm. The floorplan dimensions is 200cm x 200cm and contains 15 nodes.

Input Noise	Existing Algorithms			Novel Algorithms	
σ_d	**LSE**	**MDS**	**RQ**	**TRA**	**CIRPos**
20 cm	2.55s	0.00305s	37s	35.05s	54.25s

Table 5.9: Comparison of Computation Time for Anchor Self-Calibrating Schemes in a large area. The computation time is calculated in a simulated environment with input noise having standard deviation of 20cm. The floorplan dimensions is 4000cm x 4000cm and contains 15 nodes.

Table 5.8 and Table 5.9 show that LSE and MDS have the fastest compute times. The compute time of the novel algorithm CIRPos significantly increases as the dimensions of the indoor environment are expanded. This is because the number of floating-point calculations increases as the scale of the inter-node distances increases.

Chapter 6

Conclusion

6.1 Conclusion

We presented two novel solutions - Triangle Reconstruction Algorithm (TRA) and Channel Impulse Response Positioning (CIRPos) for anchor self-calibration in indoor environments that significantly improves the accuracy of the estimated positions as well as increases the overall anchor localization success rate of the network in noisy scenarios. We built custom calibration test setups to leverage the high accuracy ranging capability of the UWB transceivers and performed simulations to evaluate the performance characteristics of TRA and CIRPos with existing methods of anchor self-calibration.

The Triangle Reconstruction Algorithm (TRA) helps to reduce the number of robust quadrilateral "searches" required to localize a node in the network by reconstructing triangles that fail the robustness test. Nodes which are a part of only a single robust quadrilateral will recover from potential triangle inequality test failure and thereby increase the Node Localization Success Rate.

In Channel Impulse Response Positioning (CIRPos), we improved upon the Triangle Reconstruction Algorithm (TRA) by enabling the localization of orphan nodes within a network and increased both accuracy and Node Localization Success Rate by building ensuring that the algorithm is resilient to NLOS scenarios.

For future work, we are interested in developing a common protocol for which CIR metrics from different UWB hardware modules and manufacturers can be used to improve the performance of anchor self-calibration in NLOS scenarios in a hardware independent manner. This will make it easier for anchors and tags from different manufacturers to be deployed within the same indoor environment and thus increase the mass adoption of such systems.

Bibliography

[1] I. Dotlic, A. Connell, H. Ma, J. Clancy, and M. McLaughlin, "Angle of arrival estimation using decawave dw1000 integrated circuits," in *2017 14th Workshop on Positioning, Navigation and Communications (WPNC)*, 2017, pp. 1–6.

[2] Decawave, "APS011 Application Note: Sources of Error in DW1000 based Two-Way Ranging (TWR) Schemes," Dublin, Ireland, 2014, version 1.1. [Online]. Available: https://www.decawave.com/wp-content/uploads/2018/10/APS011_Sources-of-Error-in-Two-Way-Ranging-Schemes_v1.1.pdf

[3] N. Priyantha, H. R. Balakrishnan, E. D. Demaine, and S. J. Teller, "Anchor-Free Distributed Localization in Sensor Networks," 2003.

[4] Y. Liu and Z. Yang, *Location, Localization, and Localizability*. Springer New York, 2011. [Online]. Available: https://doi.org/10.1007/978-1-4419-7371-9

[5] A. A. Kannan, B. Fidan, and G. Mao, "Analysis of flip ambiguities for robust sensor network localization," *IEEE Transactions on Vehicular Technology*, vol. 59, no. 4, pp. 2057–2070, 2010.

[6] Decawave, "APS006 Part 3 Application Note: DW1000 Metrics for Estimation of Non Line of Sight Operating Conditions," Dublin, Ireland, 2016, version 1.1. [Online]. Available: https://www.decawave.com/wp-content/uploads/2018/10/APS006_Part-3-DW1000-Diagnostics-for-NLOS-Channels_v1.1.pdf

[7] ——, "APS006 Part 2 Application Note: DW1000 Metrics for Estimation of Non Line of Sight Operating Conditions," Dublin, Ireland, 2018, version 1.5. [Online]. Available: https://www.decawave.com/sites/default/files/aps006_part2_nlos_operation_and_optimizations.pdf

[8] T. Rappaport, *Wireless Communications : Principles and Practice*. Upper Saddle River, N.J: Prentice Hall PTR, 2002.

[9] Y. Huang, J. Zheng, Y. Xiao, and M. Peng, "Robust localization algorithm based on the RSSI ranging scope," *International Journal of Distributed Sensor Networks*, vol. 11, no. 2, p. 587318, Feb. 2015. [Online]. Available: https://doi.org/10.1155/2015/587318

[10] M. Cominelli, P. Patras, and F. Gringoli, "Dead on Arrival: An Empirical Study of The Bluetooth 5.1 Positioning System," in *Proceedings of the 13th International Workshop on Wireless Network Testbeds, Experimental Evaluation Characterization*, New York, NY, USA, 2019, p. 13–20.

[11] *Fundamentals of Position Location*. John Wiley Sons, Ltd, 2018, ch. One, pp. 1–2. [Online]. Available: https://onlinelibrary.wiley.com/doi/abs/10.1002/9781119434610.part1

[12] Pozyx, "How does ultra-wideband work?" [Online]. Available: https://www.pozyx.io/pozyx-academy/how-does-ultra-wideband-work

[13] L. Doherty, K. pister, and L. El Ghaoui, "Convex Position Estimation in Wireless Sensor Networks," in *Proceedings IEEE INFOCOM 2001. Conference on Computer Communications. Twentieth Annual Joint Conference of the IEEE Computer and Communications Society*, vol. 3, 2001, pp. 1655–1663 vol.3.

[14] H. T. Duong, S. Yoon, D. C. Dang, and Y. Soo Suh, "Robust Self-Calibration for Rectangle Shape UWB Anchor Locations," in *2019 IEEE SENSORS*, 2019, pp. 1–4.

[15] N. Bulusu, J. Heidemann, and D. Estrin, "Gps-less low-cost outdoor localization for very small devices," *IEEE Personal Communications*, vol. 7, no. 5, pp. 28–34, 2000.

[16] A. Savvides, C.-C. Han, and M. B. Strivastava, "Dynamic Fine-Grained Localization in Ad-Hoc Networks of Sensors," in *Proceedings of the 7th Annual International Conference on Mobile Computing and Networking*, New York, NY, USA, 2001, p. 166–179.

[17] C. Savarese, J. Rabaey, and J. Beutel, "Location in distributed ad-hoc wireless sensor networks," in *2001 IEEE International Conference on Acoustics, Speech, and Signal Processing. Proceedings*, vol. 4, 2001, pp. 2037–2040 vol.4.

[18] Y. Wang, "Linear least squares localization in sensor networks," *EURASIP Journal on Wireless Communications and Networking*, vol. 2015, no. 1, Mar. 2015. [Online]. Available: https://doi.org/10.1186/s13638-015-0298-1

[19] J. Lee, W. Chung, E. Kim, and I. W. Hong, "Robust DV-hop algorithm for localization in Wireless Sensor Network," in *ICCAS 2010*, 2010, pp. 2506–2509.

[20] K. Saneyoshi, "Drive assist system using stereo image recognition," in *Proceedings of Conference on Intelligent Vehicles*, 1996, pp. 230–235.

[21] D. Gualda, J. Ureña, J. C. García, E. García, and J. Alcalá, "Simultaneous Calibration and Navigation (SCAN) of Multiple Ultrasonic Local Positioning Systems," *Information Fusion*, vol. 45, pp. 53–65, 2019.

[22] X. Ji and H. Zha, "Sensor Positioning in Wireless Ad-Hoc Sensor Networks using Multidimensional Scaling," in *IEEE INFOCOM 2004*, 2004, pp. 2652–2661 vol.4.

[23] J. B. Saxe, "Embeddability of weighted graphs in k-space is strongly np-hard," in *Proc. of 17th Allerton Conference in Communications, Control and Computing, Monticello, IL*, 1979, pp. 480–489.

[24] T. Eren, O. Goldenberg, W. Whiteley, Y. Yang, A. Morse, B. Anderson, and P. Belhumeur, "Rigidity, computation, and randomization in network localization," in *IEEE INFOCOM 2004*, vol. 4, 2004, pp. 2673–2684 vol.4.

[25] G. Laman, "On graphs and rigidity of plane skeletal structures," *Journal of Engineering Mathematics*, vol. 4, no. 4, pp. 331–340, Oct. 1970. [Online]. Available: https://doi.org/10.1007/bf01534980

[26] B. Hendrickson, "Conditions for unique graph realizations," *SIAM J. Comput.*, vol. 21, no. 1, p. 65–84, feb 1992. [Online]. Available: https://doi.org/10.1137/0221008

[27] W. Liu, E. Dong, Y. Song, and D. Zhang, "An improved flip ambiguity detection algorithm in wireless sensor networks node localization," in *2014 21st International Conference on Telecommunications (ICT)*, 2014, pp. 206–212.

[28] W. Liu, E. Dong, and Y. Song, "A robust node localization method to address flip ambiguity in wireless networks," in *2016 International Conference on Information Networking (ICOIN)*, 2016, pp. 108–113.

[29] D. Moore, J. Leonard, D. Rus, and S. Teller, "Robust Distributed Network Localization with Noisy Range Measurements," in *Proceedings of the 2nd International Conference on Embedded Networked Sensor Systems*, New York, NY, USA, 2004, p. 50–61.

[30] M. Khamsi, *An introduction to metric spaces and fixed point theory*. New York: John Wiley, 2001.

[31] C. A. Pickover, *The math book: From pythagoras to the 57th dimension, 250 milestones in the history of Mathematics*. New York, NY: Sterling Pub, 2012.

[32] Decawave, "DW1000 User Manual: How to Use, Configure and Program the DW1000 UWB Transceiver," Dublin, Ireland, 2017, version 2.11. [Online]. Available: https://www.decawave.com/sites/default/files/resources/dw1000_user_manual_2.11.pdf

[33] ——, "APS014 Application Note: Antenna Delay Calibration of DW1000-based Products and Systems," Dublin, Ireland, 2018, version 1.2. [Online]. Available: https://www.decawave.com/wp-content/uploads/2018/10/APS014_Antennna-Delay-Calibration_V1.2.pdf

[34] ——, "DWM1001 Firmware User Guide: Based on DWM1001-DEV board," Dublin, Ireland, 2017, version 1.3. [Online]. Available: https://www.decawave.com/wp-content/uploads/2019/01/DWM1001-Firmware-User-Guide-2.1.pdf

[35] ——, "DWM1001 Firmware Application Programming(API) Guide," Dublin, Ireland, 2019, version 2.2. [Online]. Available: https://www.decawave.com/wp-content/uploads/2019/01/DWM1001-API-Guide-2.2.pdf